Attosecond Rabi oscillations in high harmonic generation resonantly driven by extreme ultraviolet laser fields

Alba de las Heras [1,2,*,†] Carlos Hernández-García [1,2] Javier Serrano [1,2] Aleksandar Prodanov,[3] Dimitar Popmintchev [4] Tenio Popmintchev [3,4] and Luis Plaja [1,2]

[1]*Grupo de Investigación en Aplicaciones del Láser y Fotónica, Departamento de Física Aplicada, Universidad de Salamanca, Salamanca E-37008, Spain*

[2]*Unidad de Excelencia en Luz y Materia Estructuradas (LUMES), Universidad de Salamanca, Salamanca, Spain*

[3]*Department of Physics, Center for Advanced Nanoscience, University of California San Diego, La Jolla, California 92093, USA*

[4]*Photonic Institute, TU Wien, Vienna A-1040, Austria*

(Received 27 March 2024; revised 12 November 2024; accepted 20 February 2025; published 16 June 2025)

High-order harmonic generation driven by intense extreme ultraviolet (EUV) fields merges quantum optics and attosecond science, giving rise to an appealing route for the generation of coherent EUV and soft x-ray light for high-resolution imaging and spectroscopies. We theoretically investigate ultrafast resonant dynamics during the interaction of He atoms with strong extreme ultraviolet pulses. At high driving intensities, we identify record fast attosecond Rabi oscillations imprinting observable signatures in the high harmonic spectrum. At field strengths suppressing the Coulomb potential barrier for all the bound states, we demonstrate the survival of the attosecond two-level dynamics for several Rabi cycles. Consequently, this intense EUV laser-atom interaction reveals a strong-field scenario in which resonant coupling of two-level bound-bound transitions prevails, in contrast to the bound-continuum transitions typically dominant in conventional infrared strong-field regimes. Our findings of a high-frequency up-conversion regime combining two coexisting pathways—a two-level coupling and a bound-continuum coupling—set an interesting perspective for extreme attosecond nonlinear optics with intense short-wavelength laser fields.

DOI: 10.1103/PhysRevResearch.7.023268

I. INTRODUCTION

The advent of high-intensity laser pulses in the extreme ultraviolet (EUV) region of the electromagnetic spectrum enables the exploration of nonlinear optics in the high-frequency regime with unprecedented attosecond temporal resolution [1,2]. Understanding attosecond extreme nonlinear optics is of interest for tracking fundamental electron-electron correlations [3–6], as well as for attosecond metrologies [7–9]. A series of breakthroughs in high-order harmonic generation (HHG) techniques to optimize the up-conversion efficiency [10–12], output power [13,14], and peak intensity [15–18] provide the appealing fully spatially and temporally coherent light to explore strong-field laser-matter interactions [19]. Remarkably, ultrafast quantum phenomena such as Rabi oscillations with periods as fast as 36 fs have been measured in the photoelectron dynamics of Ar^+ driven at EUV frequencies in a few-photon resonant interaction [20]. Also, bright EUV pulses from free-electron lasers have recently probed the resonance of autoionizing states [21] and the interference of few-photon pathways during Rabi cycles of 52 fs [22].

Among nonconventional attosecond EUV nonlinear optics phenomena, the physics of high harmonic up-conversion driven by an intense EUV pulse is yet to be fully investigated. To date, the standard approach for HHG in gases considers a lower frequency driving laser field at infrared, visible, or shorter ultraviolet wavelengths, reaching peak intensities around 10^{14}–10^{15} W/cm^2. In this range of parameters, the dominant mechanism of HHG is described by a three-step model [23,24], involving (1) tunnel ionization, (2) excursion of the electronic wave packet in the continuum, and (3) recombination with the parent ion upon the conversion of the electron kinetic energy into the emission of high-energy photons. Thus, in the low-frequency driving regime, HHG is founded in the strong coupling between the ground state and the continuum [25]. Longer wavelengths drive the electron farther apart from the parent ion and imprint more kinetic energy. As a side effect, the electron wave packet diffusion during large excursions reduces the probability of recombination [25]. Consequently, midinfrared lasers have been employed to prioritize high-photon energies [26], whereas near-ultraviolet drivers enable higher brightness [10].

For EUV drivers, the physical picture of HHG differs significantly. The tunnel ionization probability is strongly suppressed compared to multiphoton ionization [27]. Additionally, resonant electron transitions are expected to

*Contact author: albadelasheras@usal.es

†Present address: Max Planck Institute for the Structure and Dynamics of Matter and Center for Free-Electron Laser Science, Hamburg 22761, Germany.

play a relevant role, since the driving photon energies are in the order of photoexcitation energies. The few-states coupling with the laser field is characterized by a periodic electron population exchange known as Rabi oscillations [28]. Different works have unveiled femtosecond Rabi oscillations from the photoelectron spectra produced by an EUV [20,22,29–31] or near-infrared pulse [32], yet not under the conditions of full barrier suppression in the effective Coulomb potential. Rabi oscillations are relevant for identifying electron-electron correlations [33–36], for orbital angular momentum transfer from light to matter [37], for electromagnetic-induced transparency [38], or for creating population gratings [39,40]. In general, the physics of coherently driven atomic resonances itself is of a paramount research interest [41,42].

In principle, the period of Rabi oscillations can be shortened to attosecond timescales by using very intense EUV pulses. Still, an intriguing scenario arises when the electric field amplitude is large enough to deform the atomic potential leading to a transient suppression of the Coulomb barrier for all the bound states [43,44]. In this nontrivial situation, the rapid depletion of the bound electron population should affect the resonant transition, eventually dismantling the conventional coherent two-level dynamics.

In this work, we theoretically investigate the resonant electron wave packet dynamics in He atoms interacting with strong EUV laser pulses. We demonstrate the generation of high-order harmonics reaching the soft x-rays, while encoding characteristic signatures of ultrafast Rabi oscillations in both the spectral and temporal domains. We find that this extreme up-conversion is dominated by ultrafast two-state dynamics, even in the case of strong barrier suppression of all the atomic levels. Surprisingly, the two-level dynamics prevail even when the two energy levels are above the potential barrier. The perseverance of the two-level dynamics under such strong ionization conditions can be explained by considering a two-level atomic model that includes uneven level-ionization rates. The resonant interaction has a stabilizing effect, since the field-dressed states are found to ionize slower than the fastest rate of the atomic levels (see Appendix B). This coherent dressing is critical for the persistence of attosecond Rabi oscillations, since it prevents the rapid depletion of the excited state at the high driving intensities and high driving frequencies required for Rabi periods in the attosecond timescale. Unlike previous mechanisms of ionization suppression [45–50], this stabilization behavior appears exclusively in the vicinity of a resonance. In addition, our *ab initio* calculations show a substantial return of the continuum electron population to the bound states after the interaction reaches its maximum. An *ad hoc* modification of the level ionization rates to include this recombination in our two-level atomic model shows this as a second reason for the resilience of the two-level dynamics (see Appendix A).

Essentially, in this resonantly driven EUV regime, the physical description of this high-harmonic up-conversion in the sense of the conventional three steps is not possible since two different pathways coexist: (1) a two-level coupling and (2) a bound-continuum coupling. To complement our theoretical description, we provide macroscopic results of the signature of attosecond Rabi oscillations in the high harmonic spectrum at the far-field detectors considering propagation effects (see Appendix C). We foresee that high-resolution x-ray imaging as well as spectroscopic applications—using an isolated harmonic or several multicolor harmonics—may greatly benefit from this coherent soft x-ray source whose efficiency is expected to be substantially higher compared to using low-frequency drivers [10,26].

II. METHODOLOGY OF THE FIRST-PRINCIPLES CALCULATIONS

Our *ab initio* calculations describe the two-electron dynamics in a He atom along the laser polarization dimension [51]. In the numerical integration of the 1D time-dependent Schrödinger equation, we consider two active correlated electrons. Our calculations include the exact description of both neutral and ionic species, He and He^+, during the ultrafast laser interaction. The Hamiltonian in atomic units (a.u.) is given by

$$\hat{H} = \sum_{j=1}^{2}\left[\frac{1}{2}\left(\hat{p}_{x,j} + \frac{A(t)}{c}\right)^2 + V_j\right] + V_{1,2}, \tag{1}$$

where the Coulomb potentials, $V_j(x_j) = -\frac{2}{\sqrt{x_j^2+a_N}}$ and $V_{1,2}(x_1,x_2) = \frac{1}{\sqrt{(x_1-x_2)^2+a_{ee}}}$, include the softening parameters $a_{ee} = 0.32$ a.u. and $a_N = 0.50$ a.u. to match the actual ionization energies, $I_p^{He} = 24.5$ eV and $I_p^{He^+} = 54.4$ eV. $\hat{p}_{x,j} = -i\frac{\partial}{\partial x_j}$ is the momentum operator, c is the speed of light in vacuum, and $A(t)$ is the vector potential related to the electric field by $E(t) = -\frac{1}{c}\frac{\partial A(t)}{\partial t}$. The initial ground state is propagated via the finite-difference Crank-Nicolson scheme with spatial and temporal steps of $\delta x = 0.2$ a.u., and $\delta t = 0.05$ a.u. The stationary atomic states are found from the field-free Hamiltonian diagonalization. Note that the dimensional reduction and the use of the softening parameters result in energy level spacings different from the real system. Specifically, the $1s^2$–$1s2p$ resonance energy in He that we study in this work using a 1D Hamiltonian corresponds to 18.4 eV, while the same real resonant transition is expected at 21.2 eV in experiments.

We compute the dipole acceleration by applying the Ehrenfest theorem:

$$\langle a(t)\rangle = -\langle\Psi(t) \mid \nabla V(x_1,x_2) \mid \Psi(t)\rangle, \tag{2}$$

where $V(x_1,x_2) = V_1(x_1) + V_2(x_2) + V_{1,2}(x_1,x_2)$, and $\nabla = (\frac{\partial}{\partial x_1} + \frac{\partial}{\partial x_2})$. Equation (2) accounts for the total dipole emission from He and He^+, including contributions from pathways other than the two-level dynamics. To isolate the emission from the two-level dipole transition, we calculate the partial component of the acceleration

$$\langle a_{1s^2,1s2p}(t)\rangle = -c^*_{1s^2}(t)c_{1s2p}(t)\langle 1s^2 \mid \nabla V(x_1,x_2) \mid 1s2p\rangle, \tag{3}$$

where $c^*_{1s^2}(t) = \langle\Psi(t) \mid 1s^2\rangle$, and $c_{1s2p}(t) = \langle 1s2p \mid \Psi(t)\rangle$. The harmonic spectra are computed as the Fourier transform of the dipole acceleration, using Eq. (2) to obtain the total emission or Eq. (3) to select the contribution from the two-level dipole transition.

The electric field is described as a sinusoidal squared envelope of 32-cycles at the full pulse duration, $E(t) =$

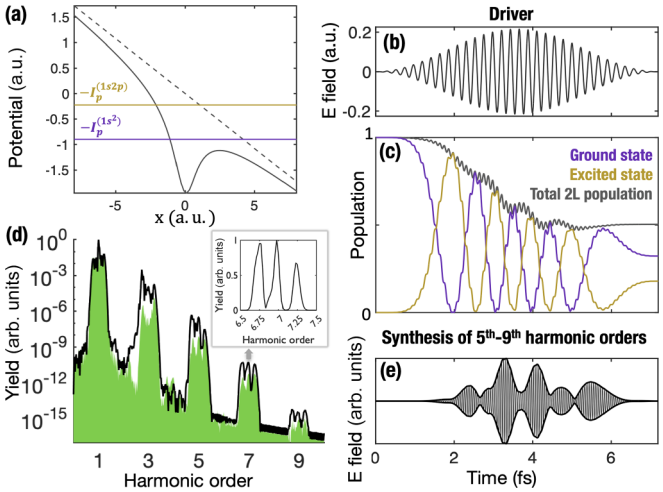

FIG. 1. (a) Effective Coulomb potential distorted by the intense EUV driving pulse, and energy levels from which the population of the $1s^2$ and $1s2p$ states ionizes: $-I_p^{(1s^2)}$ and $-I_p^{(1s2p)}$. (b) Femtosecond EUV driving electric pulse. (c) Populations of the ground state (purple) and the excited state (gold) reveal Rabi oscillations with a subfemtosecond period of ∼854 as. The total two-level population (gray) shows a steplike decay following the Rabi cycles and a certain stabilization in the second part of the interaction. (d) Corresponding high harmonic spectrum which encodes the attosecond Rabi dynamics as a characteristic three-peak structure. The black solid line is the spectrum of the total acceleration, Eq. (2), whereas the green-filled area corresponds to the contribution from the two-level dipole transition, Eq. (3). The inset shows the three-peak structure of the seventh harmonic on linear scale. (e) The synthesis of the high-order harmonics (from fifth to ninth) results in a pulse modulation on an attosecond timescale.

$E_0 \sin^2(t\omega_0/64)\sin(\omega_0 t)$. We choose driving photon energies of 12.4–24.4 eV around the atomic resonance $1s^2$–$1s2p$. The peak intensities lie in the range 8.8×10^{13}–8.8×10^{15} W/cm^2 (corresponding to field amplitudes of $E_0 = 0.05$–0.5 a.u.). This implies values of the Keldysh parameter [27] of 1.8–18.1, associated with multiphoton ionization, and corresponding to extremely short electron excursions [24] of less than 1 a.u.

III. RESULTS AND DISCUSSION

The effective Coulomb potential $V_1(x) + V_{1,2}(x, 0)$ is depicted in Fig. 1(a) at a peak intensity of 1.6×10^{15} W/cm^2 (peak field amplitude of $E_0 = 0.2154$ a.u.), where the energy levels from which the population of the resonant states ionizes, $-I_p^{(1s^2)}$ and $-I_p^{(1s2p)}$, lie above the suppressed potential barrier. Note that the potential is plotted in terms of the position of one of the electrons, x_1, while the other remains frozen at its mean position, $x_2 = 0$. It is worth pointing out that the excited level surpasses the potential barrier at lower field amplitudes than the ground state. Consequently, the excited state lies in the continuum for a longer time during the interaction with the electric EUV pulse, leading to a greater ionization compared to the ground state. This justifies the uneven ionization rates used in our two-level model presented in Appendix A. The central photon energy of the driving electric field [Fig. 1(b)] is chosen to match the atomic $1s^2$–$1s2p$ transition at 18.4 eV, corresponding to a central wavelength of 67.5 nm or a driving frequency of $\omega_0 = 0.676$ a.u.

The population of each atomic level, $1s^2$ and $1s2p$, shown in Fig. 1(c), reveals unprecedentedly rapid attosecond Rabi oscillations. The Rabi periodic modulations of ∼854 as extend over multiple Rabi cycles since the depletion of the two-level transition is on a much slower timescale of several femtoseconds. The temporal evolution of the total population occupying the atomic levels $1s^2$ and $1s2p$ is also shown in Fig. 1(c). Remarkably, half of the initial population remains in these two levels at the end of the laser pulse, despite the Coulomb barrier suppression conditions. Also, the total two-state population shows a characteristic steplike decay that follows the Rabi flopping, instead of the laser period dictating the typical strong field interaction with low-frequency infrared drivers. This suggests that the relevant modulation of the ionization is not connected with the transient suppression of the Coulomb barrier which induces a faster modulation, also observable in the calculations. Rather, the steplike dynamics are correlated with the coherent dynamics of the two-level transition. Additionally, the ionization rate is significantly reduced after the peak amplitude of the driving field is reached. All these important dynamics which are significantly different compared to the low-frequency driving regimes are further addressed in Appendix A.

In the frequency domain, the high-frequency Rabi oscillations give rise to a distinct signature in the harmonic spectrum [black solid line in Fig. 1(d)], therefore allowing for experimental characterization. Each harmonic order, q, splits into a triplet structure, where we identify the usual central peak and two additional satellite peaks at frequencies $q\omega_0 - \Omega$ and $q\omega_0 + \Omega$. Here the Rabi frequency is $\Omega \approx 0.263\,\omega_0$. The triplet structure is known to be replicated in HHG in strongly driven two-level dynamics [52,53]. In the EUV strong-field regime, the multipeak trace exhibits three well-resolved peaks of similar intensity (see the seventh harmonic on linear scale in the inset).

In addition to the analysis of the total dipole emission, the green-filled curve in Fig. 1(d) shows the harmonic spectrum associated with the two-level transition dipole, calculated using Eq. (3). We identify the two-state coupling as an important contribution to the high harmonic spectrum, exhibiting also the multipeak structure. The fact that this emission does not reproduce the full high harmonic spectrum suggests that the coupling of the resonant states with the energy continuum is also relevant in EUV-driven high harmonic generation, as expected in this high-intensity regime [54].

Interestingly, in the time domain, the synthesis of the emission from the higher-order harmonics (from fifth to ninth) yields a femtosecond pulse with an envelope that is modulated on the attosecond scale due to the Rabi flopping [Fig. 1(e)]. The yield of a two-level dipole emission is minimized when either of the two states is depleted. This introduces a prominent difference compared to the well-structured attosecond pulse trains with a half-laser-cycle period, emerging in conventional HHG from low-frequency infrared drivers [55]. This further illustrates the peculiarities of this strong-field EUV regime.

Up to this point, we have described the resonant atomic behavior. The dependence on the driving photon energy is shown

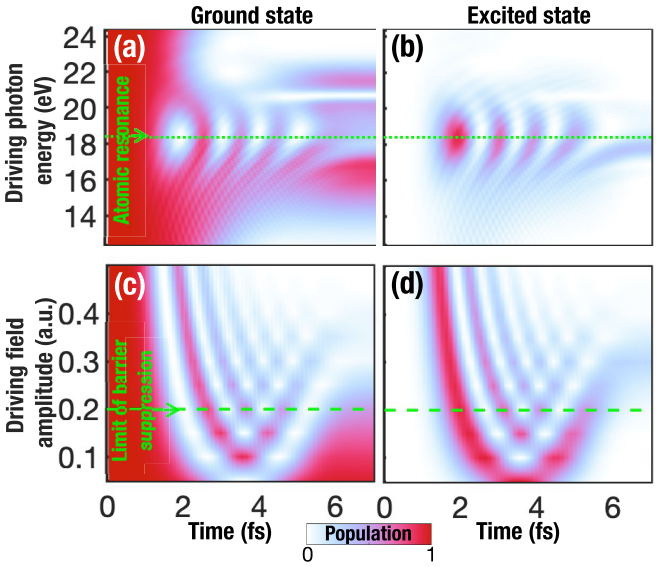

FIG. 2. Ultrafast evolution of the populations of (a) the ground state and (b) the excited state of He for different driving photon energies at a peak intensity of $1.6 \times 10^{15}\,\mathrm{W/cm^2}$, illustrating femtosecond-to-attosecond Rabi oscillations in a broad range of photon energies around the resonance. Panels (c) and (d) show the direct increase of the frequency of the Rabi oscillations to attosecond timescales (to sub-500 as) with the driving field amplitude for the resonant case of 18.4 eV.

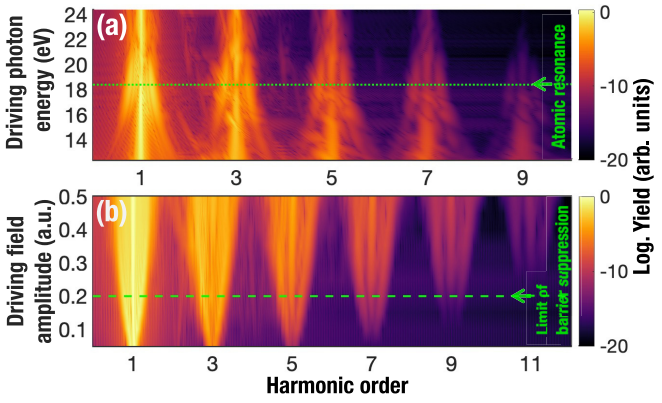

FIG. 3. (a) High harmonic spectrum as a function of the driving photon energy at a fixed peak intensity of $1.6 \times 10^{15}\,\mathrm{W/cm^2}$, showing the well-pronounced three-peak spectroscopic signature of the attosecond Rabi oscillations at resonance. (b) High harmonic spectrum as a function of the driving field amplitude at the resonant photon energy of 18.4 eV.

in Figs. 2(a) and 2(b), while the peak intensity is maintained at $1.6 \times 10^{15}\,\mathrm{W/cm^2}$. We observe attosecond Rabi oscillations in the populations of the ground [Fig. 2(a)] and excited [Fig. 2(b)] states in the vicinity of the atomic resonance (indicated with a green dotted line). The frequency of the Rabi oscillations increases with the detuning between the driving field frequency (ω_0) and the frequency of the atomic transition (ω_a), $\Delta = \omega_a - \omega_0$. This is in agreement with the equation of the generalized Rabi frequency in a two-level system [56]: $\Omega = \sqrt{\Delta^2 + |\chi|^2}$, where $|\chi|^2$ is the intensity of the coupling, and the longest Rabi period corresponds to the resonant case $\Delta = 0$. Still, a slight energy shift of the resonant transition ($\sim$1 eV) arises during the interaction with the laser pulse, most probably resulting from the field dressing.

We also note that the total two-state population remarkably depends on the driving photon energy [Figs. 2(a) and 2(b)]. There is a strong depletion far away from the resonance, whereas the two-level population exhibits stabilized dynamics for small detunings. Intriguingly, the behavior is not symmetric for positive and negative detunings. At photon energies slightly below the resonance, the population is more stable. By introducing a certain detuning, the Rabi oscillations become less efficient in the population transfer to the excited state—which has a higher ionization rate $\gamma_2(t) > \gamma_1(t)$—so one would expect a lower depletion of the total two-level population, as observed for small positive detunings. In contrast, at slightly higher energies above the resonance, we notice narrow channels of strong and low depletion that might be attributed to other atomic resonances.

The scaling of the evolution of the population with the driving field amplitude [Figs. 2(c) and 2(d)] also deserves special attention. Increasing the field amplitude implies more ionization and faster Rabi oscillations. The two effects are expected since (1) we are enhancing the bound-continuum coupling and (2) the Rabi frequency is directly proportional to the amplitude of the resonant driver [56]. Note the pronounced ionization only occurs well beyond the limit of barrier suppression for all bound states, which again suggests that the reduction of the ionization rate is due to resonant stabilization. This fact is of paramount importance for the persistence of Rabi oscillations with periods even shorter than 500 as.

Moving once again to the frequency domain, the high harmonic spectrum in Fig. 3(a) presents a map of the satellite-peak structure around the resonance [also shown in Fig. 1(d)]. Similar to the two-level picture, we recover the single peak far off resonance. This wide range of detunings at which Rabi oscillations can be observed should ease the experimental traceability of these two-level coherent dynamics in He in the strong high-frequency interaction regime.

As the EUV field amplitude increases [see Fig. 3(b)], the satellite peaks in the high harmonic spectrum separate, also as expected for a two-level system. Despite the depletion of the bound states, the HHG efficiency rises for stronger field amplitudes and the multipeak signature is preserved. The harmonic signal is observed up to the eleventh harmonic, corresponding to a soft x-ray photon energy of 202 eV. A closer inspection of Fig. 3(b) indicates that the relevance of the central harmonic peak increases at higher driving intensities. This suggests that its origin is associated with the bound-continuum coupling, instead of the two-level transition (as further corroborated in Appendix A).

IV. CONCLUSIONS

In summary, we have studied the generation of high-order harmonics using an EUV driver both as an alternative soft x-ray coherent source and as a powerful spectroscopic tool. Our *ab initio* calculations reveal attosecond Rabi oscillations

in the resonant dynamics of EUV-driven HHG. To the best of our knowledge, these are the fastest Rabi oscillations ever reported. Despite the high EUV intensities required to reach Rabi periods in the attosecond scale, the coupled two-state behavior survives during the strong field interaction. Using a simplified two-level model including uneven level-ionization rates, we demonstrate that the dressed states deplete at a slower ionization rate than the fastest rate of the bare states, stabilizing the coupled two-state population. The signature of the ultrafast Rabi oscillations is uniquely encoded in the EUV-driven high harmonic spectrum as a multipeak harmonic structure, allowing for experimental characterization. In Appendix C we demonstrate that the spectroscopic trace is preserved after propagation towards the far-field detectors. We also observe a larger divergence of the satellites compared to the main peaks due to the different physical origins of the emission.

We envision EUV strong-field interactions as a new fascinating area of extreme nonlinear optics and attosecond quantum optics radically different from its lower-frequency counterpart, now accessible with cutting-edge high harmonic sources and EUV free-electron lasers. Further optimization of this EUV-driven HHG regime could provide a bright coherent light source enhancing the capabilities of high-resolution imaging and spectroscopy in the soft x-ray photon energy range. In the case of EUV drivers, phase matching can be achieved at a large range of pressures paving the way for higher brightness. In addition, the photon energies of the generated harmonics are high enough to access core or semicore electron dynamics, and the higher separation in photon energies of different harmonics simplifies the filtering of single harmonics for yielding quasimonochromatic sources.

ACKNOWLEDGMENTS

We acknowledge funding from the European Research Council (ERC) under the European Union's Horizon 2020 research and innovation program (Grant Agreement No. 851201), as well as from the Project No. PID2022-142340NB-I00 financed by Ministerio de Ciencia e Innovacción and Agencia Estatal de Investigación (MCIN/AEI/10.13039/501100011033/). T.P. acknowledges funding from the European Research Council (ERC) under the European Union's Horizon 2020 research and innovation program (Grant Agreement No. XSTREAM-716950), from the Alfred P. Sloan Foundation (FG-2018-10892), and from University of California San Diego Startup Funding. The authors also acknowledge the resources from the supercomputer SCAYLE and the Spanish Supercomputing Network (FI-2022-3-0041). The authors acknowledge TU Wien Bibliothek for financial support through its Open Access Funding Programme.

DATA AVAILABILITY

The data supporting the findings of this study is available in the main text and appendices of this article. Additional data is available from the authors upon reasonable request.

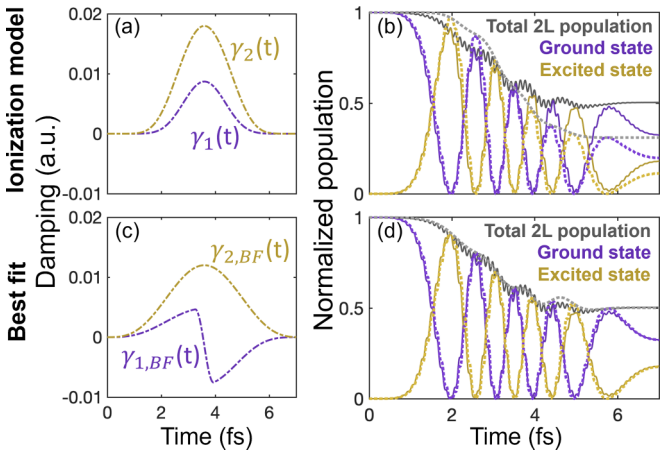

FIG. 4. (a) Ionization rates of the ground (purple) and excited (gold) state using the theory of Ref. [54]. (b) Comparison of the evolution of the population of the states obtained using the two-level model (dashed lines) versus the *ab initio* TDSE description (solid lines), showing identical periods of Rabi oscillation, while the ionization rates are overestimated by the two-level model. (c) and (d) Comparison of the equivalent plots using a best-fit two-level model versus the exact TDSE solution showing an excellent agreement in ionization rates. We consider a resonant EUV driving pulse with a central photon energy of $\omega_0 = \omega_a = 18.4$ eV and a peak intensity of 1.6×10^{15} W/cm^2.

APPENDIX A: TWO-LEVEL MODEL WITH UNEVEN IONIZATION RATES

We consider the equations of the dynamics in a two-level system featuring uneven damping functions $\gamma_1(t)$ and $\gamma_2(t)$:

$$\dot{c}_1(t) = -\frac{i}{2}\{-[\omega_a + i\gamma_1(t)]c_1(t) - [\chi(t)e^{-i\omega_0 t} + \chi^*(t)e^{i\omega_0 t}]c_2(t)\}, \quad \text{(A1)}$$

$$\dot{c}_2(t) = -\frac{i}{2}\{[\omega_a - i\gamma_2(t)]c_2(t) - [\chi(t)e^{-i\omega_0 t} + \chi^*(t)e^{i\omega_0 t}]c_1(t)\}. \quad \text{(A2)}$$

Here the driving laser frequency is denoted as ω_0, and the atomic transition frequency as ω_a. The coupling strength is modeled as $\chi(t) = \chi_0\,\mathrm{Env}(t)$, with $\chi_0 = 0.178$ a.u. being the peak coupling strength, and $\mathrm{Env}(t) = \sin^2(t\omega_0/64)$ the driving pulse envelope of 32 cycles full duration. The numerical solution of Eqs. (A1) and (A2) is found using a standard Runge-Kutta method.

First, we estimate $\gamma_1(t)$ and $\gamma_2(t)$ using the model in Ref. [54] to mimic the standard ionization from each level [see Fig. 4(a)]. Figure 4(b) shows the comparison of the population evolution in the two-level model (2L model in dashed lines) and the full time-dependent Schrödinger equation (full TDSE in solid lines). While this simplified 2L theoretical description perfectly reproduces the frequency of the Rabi oscillations obtained with the TDSE model, the population decay is overestimated.

As an alternative method to evaluate the damping functions, we perform best-fit analyses (2L-BF) to match the full TDSE calculations by tuning the damping functions $\gamma_{1,BF}(t)$

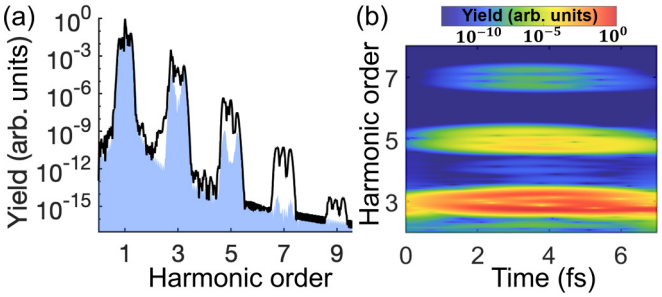

FIG. 5. (a) Comparison of EUV-driven high harmonic spectra obtained using the 2L two-level model (blue area), compared to the exact TDSE calculation (black line). The strong coupling to the continuum states for the higher order harmonics (fifth, seventh) is indicated by their reduced intensity and the absent central peak. (b) Time-frequency analysis of the full TDSE calculation shows that the emission of the central peaks occurs later in the interaction in contrast to the satellite peaks. The driving laser parameters are the same as in Fig. 4.

and $\gamma_{2,BF}(t)$ [see Fig. 4(c)]. A key element here is to include the return of the population to the bound states. Since the electron dynamics driven by EUV pulses occur in short spatial distances, the dressed states remain in the atomic vicinity as stable virtual states. Then the electron population excited to higher Rydberg and continuum states are expected to play a fundamental role as a reservoir of probability, which is injected into the two-level states after the driving field's maximum. In the damping functions $\gamma_{1,BF}(t)$ and $\gamma_{2,BF}(t)$ shown in Fig. 4(c), we consider both the ionization rate, as well as the recombination mechanism that increases the two-level population later in the interaction. Note that $\gamma_{1,BF}(t)$ flips its sign after the maximum of the driving pulse envelope. The excellent agreement of this 2L-BF model with the exact TDSE calculations is shown in Fig. 4(d), indicating that the return of electron population from higher Rydberg and continuum states to the two-level system effectively reverses the ionization depletion during the interaction with the laser field.

We compute the 2L dipole spectrum as $\mathrm{Re}\{c_1(t)c_2^*(t)\}$. The high harmonic spectrum from the *ab initio* TDSE calculation is shown in black in Fig. 5(a), whereas the blue area corresponds to the 2L model with the standard ionization rates $\gamma_1(t)$ and $\gamma_2(t)$. We checked that the reduced population of this 2L model (which neglects the population return) does not lead to a significant change in the spectral shape. Instead, the much lower yield of the higher order harmonics (seventh, ninth) resulting from the two-level calculation can be attributed to the strong coupling with the continuum, which amplifies the high-frequency dipole emission. Note also that the position of the satellite peaks is perfectly matched, while the absence of the central peak in the 2L model is another indication of the relevance of the coupling to the continuum. The time-frequency analysis of the full TDSE calculation shown in Fig. 5(b) reveals that the emission of the central peaks occurs later in the interaction than the satellite peaks. This is also consistent with the interpretation of the central peak as an effect of bound-continuum coupling, as only the satellite peaks are observed at early times of the laser interaction when the continuum is still not populated.

The comparison between the full TDSE and the 2L spectra in Fig. 5(a) demonstrates that EUV-driven HHG cannot be understood from the standard isolated resonant two-level dynamics since, for our laser field parameters, the dressed atomic levels have energies above the Coulomb barrier, implying that the electron wave packet is no longer bound. The bound-continuum coupling amplifies the emission of higher harmonic orders reaching soft x-ray photon energies. Still, it also becomes evident that the physical mechanism of HHG resonantly driven by EUV pulses cannot be understood with the standard three-step model that applies to conventional infrared drivers, since the short-scale electron dynamics would not map into soft x-ray photon energies upon recombination to the parent ion and only two-level dynamics can explain the emergence of satellite peaks. This process of EUV-driven HHG can only be interpreted in a joint picture accounting for two-level dynamics and bound-continuum coupling, which intertwines the areas of quantum optics and extreme strong-field physics.

APPENDIX B: DRESSED EIGENVALUES IN THE ROTATING WAVE APPROXIMATION

The ionization rates presented in Figs. 4(a) and 4(c) have a pronounced asymmetry ($\gamma_2 \gg \gamma_1$). Naively, it might seem that the average lifetime of the two-level transition would be predominantly influenced by the quickest ionization process, namely, the ionization of the excited state, characterized by a mean ionization time $\overline{\tau}_2 = 1/\overline{\gamma}_2 \sim 4.8$ fs. Figures 4(b) and 4(c) demonstrate that this is not the case, as the Rabi oscillations extend over a time much larger than $\overline{\tau}_2$. We resort to the dressed-state picture to understand this robust stabilization dynamics of the two-level transition with respect to ionization.

The energy of the dressed levels can be computed by diagonalizing the rotating-wave approximated (RWA) Hamiltonian:

$$H_{\mathrm{RWA}} = \frac{1}{2}\begin{pmatrix} -\Delta_1'(t) & -\chi^*(t) \\ -\chi(t) & \Delta_2'^*(t) \end{pmatrix}, \tag{B1}$$

which is non-Hermitian due to the inclusion of the ionization dynamics. The complex detunings are defined as $\Delta_1' = \Delta + i\gamma_1(t)$ and $\Delta_2' = \Delta + i\gamma_2(t)$, where $\Delta = \omega_a - \omega_0$. The Hamiltonian diagonalization leads to two complex-valued dressed state energies $\lambda_-(t)$ and $\lambda_+(t)$:

$$\lambda_\pm(t) = \frac{\overline{\gamma}(t)}{2}\left\{-i \pm \left[\left(\frac{\Delta}{\overline{\gamma}(t)} - i\alpha(t)\right)^2 + \frac{|\chi(t)|^2}{\overline{\gamma}(t)^2}\right]^{1/2}\right\} \tag{B2}$$

where $\overline{\gamma}(t) = [\gamma_1(t) + \gamma_2(t)]/2$, and the γ-asymmetry factor is defined as $\alpha(t) = [\gamma_2(t) - \gamma_1(t)]/[\gamma_2(t) + \gamma_1(t)]$. Considering the parameter space of our EUV strong-field interaction, the first term is the dominant one. Hence, the population decay of the dressed eigenstates is essentially dominated by $\overline{\gamma}(t)$. The γ-asymmetry explains the steplike damping of the Rabi oscillations in Fig. 4(d), in both the *ab initio* TDSE and 2L-BF descriptions. A more substantial depletion occurs at the Rabi half periods where the population is mainly in the excited state, contrasting with the lower depletion when the

ground state is highly populated. Consequently, the total 2L population which is periodically exchanged between the two states depletes with $\overline{\gamma}(t)$.

The generalized Rabi frequency can be expressed as

$$\Omega(t) = \mathrm{Re}\{\lambda_+(t) - \lambda_-(t)\} = \mathrm{Re}\Big\{\sqrt{(\Delta - i\alpha(t)\overline{\gamma}(t))^2 + |\chi(t)|^2}\Big\}, \tag{B3}$$

which in the case of even damping, i.e., $\gamma_1(t) = \gamma_2(t)$, reduces to

$$\Omega(t) = \sqrt{\Delta^2 + |\chi(t)|^2}. \tag{B4}$$

APPENDIX C: HIGH HARMONIC SPECTROSCOPIC SIGNATURES AT FAR-FIELD DETECTORS

We address the macroscopic point of view by providing numerical results of EUV resonantly driven HHG from a He gas target. The calculations are performed in the framework of the discrete dipole approximation [57] by considering elementary dipole emitters at a transverse generation plane. At the single-atom level, we model the interaction with the *ab initio* TDSE description described in the methods section. Then, the Maxwell propagator is applied to obtain the high harmonic beam at a far-field detector [57]. With this theoretical approach, we simulate the effect of transverse phase matching [58], which has been demonstrated as the dominant propagation effects in HHG experiments under loose focusing conditions in low-density gas mediums even for large interaction lengths [59].

The spatial profile of the driver is modeled as a Gaussian beam with waist of 50 µm and a high peak intensity of $2.2 \times 10^{15}\,\mathrm{W/cm^2}$. We keep the temporal envelope of the single-atom calculations and a central photon energy of 18.4 eV to match the resonance. The results of the far-field high harmonic beam at the detector are shown in Fig. 6. Figure 6(a) depicts the integrated high harmonic spectrum,

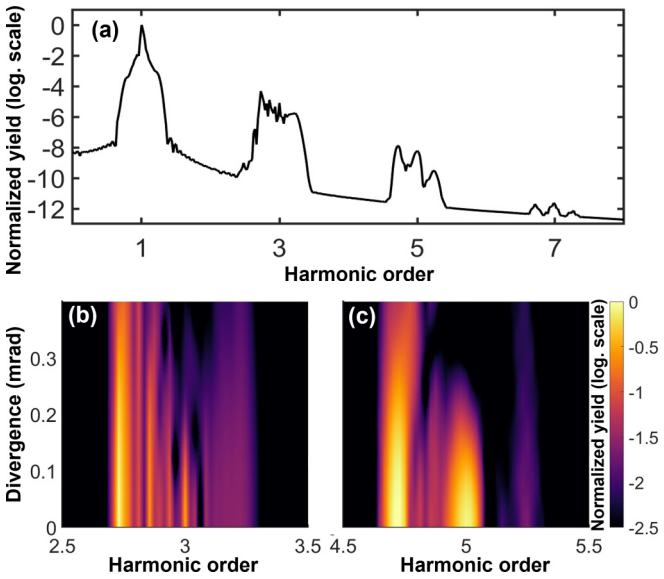

FIG. 6. Far-field high harmonic signatures of attosecond Rabi oscillations from a He gas target considering the effect of transverse phase matching and propagation to the detector. We depict (a) the integrated high harmonic spectrum with preserved three-peak structure and the dependence of the spatial profile in the vicinity of (b) the third and (c) fifth harmonic orders indicating larger divergence of the satellites versus the main peak due to the different physical origin.

where the multi-peak trace is clearly observable in the generated harmonics. Figures 6(b) and 6(c) represent the radial divergence of the harmonic beam in the vicinity of the third and fifth harmonics, respectively. Interestingly, the central peak is confined to a smaller spot than the satellite peaks, which extend to larger divergence angles. This can be interpreted as another manifestation of the different mechanism originating the satellite peaks (dressed two-level dynamics) and the central peak (ground-continuum coupling). The measurement of this feature would be a robust experimental spectroscopic signature of attosecond Rabi oscillations.

[1] G. Sansone, L. Poletto, and M. Nisoli, High-energy attosecond light sources, Nat. Photon. **5**, 655 (2011).

[2] J. Duris, S. Li, T. Driver, E. G. Champenois, J. P. MacArthur, A. A. Lutman, Z. Zhang, P. Rosenberger, J. W. Aldrich, R. Coffee *et al.*, Tunable isolated attosecond X-ray pulses with gigawatt peak power from a free-electron laser, Nat. Photon. **14**, 30 (2020).

[3] Y. Nabekawa, H. Hasegawa, E. J. Takahashi, and K. Midorikawa, Production of doubly charged helium ions by two-photon absorption of an intense sub-10-fs soft x-ray pulse at 42 eV photon energy, Phys. Rev. Lett. **94**, 043001 (2005).

[4] K. Midorikawa, Y. Nabekawa, and A. Suda, XUV multiphoton processes with intense high-order harmonics, Prog. Quantum Electron. **32**, 43 (2008).

[5] P. Tzallas, E. Skantzakis, L. A. A. Nikolopoulos, G. D. Tsakiris, and D. Charalambidis, Extreme-ultraviolet pump–probe studies of one-femtosecond-scale electron dynamics, Nat. Phys. **7**, 781 (2011).

[6] M. Kretschmar, A. Hadjipittas, B. Major, J. Tümmler, I. Will, T. Nagy, M. J. J. Vrakking, A. Emmanouilidou, and B. Schütte, Attosecond investigation of extreme-ultraviolet multi-photon multi-electron ionization, Optica **9**, 639 (2022).

[7] P. Tzallas, D. Charalambidis, N. A. Papadogiannis, K. Witte, and G. D. Tsakiris, Direct observation of attosecond light bunching, Nature **426**, 267 (2003).

[8] T. Sekikawa, A. Kosuge, T. Kanai, and S. Watanabe, Nonlinear optics in the extreme ultraviolet, Nature **432**, 605 (2004).

[9] I. Orfanos, I. Makos, I. Liontos, E. Skantzakis, B. Förg, D. Charalambidis, and P. Tzallas, Attosecond pulse metrology, APL Photon. **4**, 080901 (2019).

[10] D. Popmintchev, C. Hernandez-Garcia, F. Dollar, C. Mancuso, J. A. Perez-Hernandez, M.-C. Chen, A. Hankla, X. Gao, B. Shim, A. L. Gaeta *et al.*, Ultraviolet surprise: Efficient soft x-ray high-harmonic generation in multiply ionized plasmas, Science **350**, 1225 (2015).

[11] H. Wang, Y. Xu, S. Ulonska, J. S. Robinson, P. Ranitovic, and R. A. Kaindl, Bright high-repetition-rate source of narrowband extreme-ultraviolet harmonics beyond 22 eV, Nat. Commun. **6**, 7459 (2015).

[12] F. Ferrari, F. Calegari, M. Lucchini, C. Vozzi, S. Stagira, G. Sansone, and M. Nisoli, High-energy isolated attosecond pulses generated by above-saturation few-cycle fields, Nat. Photon. **4**, 875 (2010).

[13] E. J. Takahashi, P. Lan, O. D. Mücke, Y. Nabekawa, and K. Midorikawa, Attosecond nonlinear optics using gigawatt-scale isolated attosecond pulses, Nat. Commun. **4**, 2691 (2013).

[14] B. Xue, Y. Tamaru, Y. Fu, H. Yuan, P. Lan, O. D. Mücke, A. Suda, K. Midorikawa, and E. J. Takahashi, Fully stabilized multi-TW optical waveform synthesizer: Toward gigawatt isolated attosecond pulses, Sci. Adv. **6**, aay2802 (2020).

[15] H. Mashiko, A. Suda, and K. Midorikawa, Focusing coherent soft-x-ray radiation to a micrometer spot size with an intensity of 10^{14} W/cm^2, Opt. Lett. **29**, 1927 (2004).

[16] B. Bergues, D. E. Rivas, M. Weidman, A. A. Muschet, W. Helml, A. Guggenmos, V. Pervak, U. Kleineberg, G. Marcus, R. Kienberger *et al.*, Tabletop nonlinear optics in the 100-eV spectral region, Optica **5**, 237 (2018).

[17] B. Major, O. Ghafur, K. Kovács, K. Varjú, V. Tosa, M. J. J. Vrakking, and B. Schütte, Compact intense extreme-ultraviolet source, Optica **8**, 960 (2021).

[18] B. Senfftleben, M. Kretschmar, A. Hoffmann, M. Sauppe, J. Tümmler, I. Will, T. Nagy, M. J. Vrakking, D. Rupp, and B. Schütte, Highly non-linear ionization of atoms induced by intense high-harmonic pulses, J. Phys.: Photon. **2**, 034001 (2020).

[19] X. Shi, C.-T. Liao, Z. Tao, E. Cating-Subramanian, M. M. Murnane, C. Hernández-García, and H. C. Kapteyn, Attosecond light science and its application for probing quantum materials, J. Phys. B: At. Mol. Opt. Phys. **53**, 184008 (2020).

[20] M. Flögel, J. Durá, B. Schütte, M. Ivanov, A. Rouzée, and M. J. J. Vrakking, Rabi oscillations in extreme ultraviolet ionization of atomic argon, Phys. Rev. A **95**, 021401(R) (2017).

[21] C. Ott, L. Aufleger, T. Ding, M. Rebholz, A. Magunia, M. Hartmann, V. Stooß, D. Wachs, P. Birk, G. D. Borisova *et al.*, Strong-field extreme-ultraviolet dressing of atomic double excitation, Phys. Rev. Lett. **123**, 163201 (2019).

[22] S. Nandi, E. Olofsson, M. Bertolino, S. Carlström, F. Zapata, D. Busto, C. Callegari, M. Di Fraia, P. Eng-Johnsson, R. Feifel *et al.*, Observation of Rabi dynamics with a short-wavelength free-electron laser, Nature **608**, 488 (2022).

[23] K. J. Schafer, B. Yang, L. F. DiMauro, and K. C. Kulander, Above threshold ionization beyond the high harmonic cutoff, Phys. Rev. Lett. **70**, 1599 (1993).

[24] P. B. Corkum, Plasma perspective on strong field multiphoton ionization, Phys. Rev. Lett. **71**, 1994 (1993).

[25] M. Lewenstein, P. Balcou, M. Y. Ivanov, A. L'Huillier, and P. B. Corkum, Theory of high-harmonic generation by low-frequency laser fields, Phys. Rev. A **49**, 2117 (1994).

[26] T. Popmintchev, M. C. Chen, D. Popmintchev, P. Arpin, S. Brown, S. Ališauskas, G. Andriukaitis, T. Balčiunas, O. D. Mücke, A. Pugzlys *et al.*, Bright coherent ultrahigh harmonics in the keV x-ray regime from mid-infrared femtosecond lasers, Science **336**, 1287 (2012).

[27] L. V. Keldysh, Ionization in the field of a strong electromagnetic wave, Sov. Phys. JETP **20**, 1307 (1965).

[28] I. I. Rabi, On the process of space quantization, Phys. Rev. **49**, 324 (1936).

[29] W. C. Jiang, H. Liang, S. Wang, L. Y. Peng, and J. Burgdörfer, Enhancing Autler-Townes splittings by ultrafast XUV pulses, Phys. Rev. Res. **3**, L032052 (2021).

[30] E. Olofsson and J. M. Dahlström, Photoelectron signature of dressed-atom stabilization in an intense XUV field, Phys. Rev. Res. **5**, 043017 (2023).

[31] F. Richter, U. Saalmann, E. Allaria, M. Wollenhaupt, B. Ardini, A. Brynes, C. Callegari, G. Cerullo, M. Danailov, A. Demidovich, K. Dulitz, R. Feifel, M. di Fraia, S. D. Ganeshamandiram, L. Giannessi, N. Gölz, S. Hartweg, B. von Issendorff, T. Laarmann *et al.*, Strong-field quantum control in the extreme ultraviolet domain using pulse shaping, Nature **636**, 337 (2024).

[32] M. Fushitani, C.-N. Liu, A. Matsuda, T. Endo, Y. Toida, M. Nagasono, T. Togashi, M. Yabashi, T. Ishikawa, Y. Hikosaka *et al.*, Femtosecond two-photon Rabi oscillations in excited He driven by ultrashort intense laser fields, Nat. Photon. **10**, 102 (2016).

[33] Q. Liao, Y. Zhou, C. Huang, and P. Lu, Multiphoton Rabi oscillations of correlated electrons in strong-field nonsequential double ionization, New J. Phys. **14**, 013001 (2012).

[34] Y. O. Dudin, L. Li, F. Bariani, and A. Kuzmich, Observation of coherent many-body Rabi oscillations, Nat. Phys. **8**, 790 (2012).

[35] U. De Giovannini, G. Brunetto, A. Castro, J. Walkenhorst, and A. Rubio, Simulating pump-probe photoelectron and absorption spectroscopy on the attosecond timescale with time-dependent density functional theory, ChemPhysChem **14**, 1363 (2013).

[36] Y. Chen, Y. Zhou, Y. Li, M. Li, P. Lan, and P. Lu, Rabi oscillation in few-photon double ionization through doubly excited states, Phys. Rev. A **97**, 013428 (2018).

[37] C. T. Schmiegelow, J. Schulz, H. Kaufmann, T. Ruster, U. G. Poschinger, and F. Schmidt-Kaler, Transfer of optical orbital angular momentum to a bound electron, Nat. Commun. **7**, 12998 (2016).

[38] P. Ranitovic, X. M. Tong, C. W. Hogle, X. Zhou, Y. Liu, N. Toshima, M. M. Murnane, and H. C. Kapteyn, Controlling the XUV transparency of helium using two-pathway quantum interference, Phys. Rev. Lett. **106**, 193008 (2011).

[39] R. M. Arkhipov, Population gratings created by a pair of unipolar attosecond pulses in a three-level atomic medium, Opt. Spectrosc. **128**, 1865 (2020).

[40] R. Arkhipov, A. Pakhomov, M. Arkhipov, I. Babushkin, A. Demircan, U. Morgner, and N. Rosanov, Population difference gratings created on vibrational transitions by nonoverlapping subcycle THz pulses, Sci. Rep. **11**, 1961 (2021).

[41] V. Strelkov, Role of autoionizing state in resonant high-order harmonic generation and attosecond pulse production, Phys. Rev. Lett. **104**, 123901 (2010).

[42] A. Kaldun, A. Blättermann, V. Stooß, S. Donsa, H. Wei, R. Pazourek, S. Nagele, C. Ott, C. D. Lin, J. Burgdörfer, and T. Pfeifer, Observing the ultrafast buildup of a Fano resonance in the time domain, Science **354**, 738 (2016).

[43] S. Augst, D. Strickland, D. D. Meyerhofer, S. L. Chin, and J. H. Eberly, Tunneling ionization of noble gases in a high-intensity laser field, Phys. Rev. Lett. **63**, 2212 (1989).

[44] S. Augst, D. D. Meyerhofer, D. Strickland, and S. L. Chint, Laser ionization of noble gases by Coulomb-barrier suppression, J. Opt. Soc. Am. B **8**, 858 (1991).

[45] R. J. Vos and M. Gavrila, Effective stabilization of Rydberg states at current laser performances, Phys. Rev. Lett. **68**, 170 (1992).

[46] J. H. Eberly and K. C. Kulander, Atomic stabilization by superintense lasers, Science **262**, 1229 (1993).

[47] I. P. Christov, J. Zhou, J. Peatross, A. Rundquist, M. M. Murnane, and H. C. Kapteyn, Nonadiabatic effects in high-harmonic generation with ultrashort pulses, Phys. Rev. Lett. **77**, 1743 (1996).

[48] A. M. Popov, O. V. Tikhonova, and E. A. Volkova, Strong-field atomic stabilization: Numerical simulation and analytical modelling, J. Phys. B: At. Mol. Opt. Phys. **36**, R125 (2003).

[49] U. Eichmann, A. Saenz, S. Eilzer, T. Nubbemeyer, and W. Sandner, Observing Rydberg atoms to survive intense laser fields, Phys. Rev. Lett. **110**, 203002 (2013).

[50] Q. Wei, P. Wang, S. Kais, and D. Herschbach, Pursuit of the Kramers-Henneberger atom, Chem. Phys. Lett. **683**, 240 (2017).

[51] A. de las Heras, C. Hernández-García, and L. Plaja, Spectral signature of back reaction in correlated electron dynamics in intense electromagnetic fields, Phys. Rev. Res. **2**, 033047 (2020).

[52] L. Plaja and L. Roso-Franco, Adiabatic theory for high-order harmonic generation in a two-level atom, J. Opt. Soc. Am. B **9**, 2210 (1992).

[53] A. Picón, L. Roso, J. Mompart, O. Varela, V. Ahufinger, R. Corbalán, and L. Plaja, Dipole spectrum structure of nonresonant nonpertubative driven two-level atoms, Phys. Rev. A **81**, 033420 (2010).

[54] S. V. Popruzhenko, V. D. Mur, V. S. Popov, and D. Bauer, Strong field ionization rate for arbitrary laser frequencies, Phys. Rev. Lett. **101**, 193003 (2008).

[55] P. M. Paul, E. S. Toma, P. Breger, G. Mullot, F. Augé, P. Balcou, H. G. Muller, and P. Agostini, Observation of a train of attosecond pulses from high harmonic generation, Science **292**, 1689 (2001).

[56] C. J. Joachain, N. J. Kylstra, and R. M. Potvliege, *Atoms in Intense Laser Fields* (Cambridge University Press, Cambridge, 2011).

[57] C. Hernández-García, J. A. Pérez-Hernández, J. Ramos, E. C. Jarque, L. Roso, and L. Plaja, High-order harmonic propagation in gases within the discrete dipole approximation, Phys. Rev. A **82**, 033432 (2010).

[58] C. Hernández-García, I. J. Sola, and L. Plaja, Signature of the transversal coherence length in high-order harmonic generation, Phys. Rev. A **88**, 043848 (2013).

[59] A. K. Pandey, A. de las Heras, T. Larrieu, J. S. Román, J. Serrano, L. Plaja, E. Baynard, M. Pittman, G. Dovillaire, S. Kazamias *et al.*, Characterization of extreme ultraviolet vortex beams with a very high topological charge, ACS Photon. **9**, 944 (2022).